

Analysis of Neutron Star f -mode Oscillations in General Relativity with Spectral Representation of Nuclear Equations of State

DEBANJAN GUHA ROY,¹ TUHIN MALIK,² SWASTIK BHATTACHARYA,¹ AND SARMISTHA BANIK¹

¹*Department of Physics, Birla Institute of Technology and Science Pilani, Hyderabad Campus, Telangana 500078, India.*

²*CFisUC, Department of Physics, University of Coimbra, 3004-516 Coimbra, Portugal.*

ABSTRACT

We conduct a detailed analysis of quasinormal f -mode frequencies in neutron stars (NS), within the linearized General Relativistic formalism. From Bayesian inference, we derived approximately 9000 nuclear Equations of State (EOS) subject to various constraints including nuclear saturation properties, the pure neutron matter EOS constraint obtained within χ EFT, and pQCD at densities relevant to NS cores. The composition and oscillatory dynamics of NS are then investigated using this set. The EOS are transformed into a spectral representation, aiding in the efficient computation of NS properties. The median frequency values of the f -mode for NS with masses ranging from $1.4M_{\odot}$ to $2.0M_{\odot}$ lie between 1.80 and 2.20 kHz for our entire EOS set. Our findings do not reveal a strong correlation between f -mode frequencies and individual nuclear saturation properties of the EOS. This suggests the need for more complex methods to unravel multiple-parameter relationships. We noticed a strong relationship between the radii and f -mode frequencies for different NS masses. Using this correlation along with NICER observations of PSR J0740+6620 and PSR 0030+0451, we obtained constraints that have minimal overlap in the radius domain and differ in the frequency domain from our entire nucleonic EOS set. This indicates that there may be a need to consider additional exotic particles or maybe a deconfined quark phase in the EOS relevant to the NS core. We argue that future observations of the radius or f -mode frequency for more than one NS mass, particularly at the extremes, are likely to settle the issue by either ruling out only nucleonic EOS or providing definitive evidence in its favour.

Keywords: Neutron star, Dense matter, Equation of State, Quasi-static oscillation, Quasinormal modes, f -modes, Perturbative QCD, Spectral representation, Relativistic mean field model

1. INTRODUCTION

Neutron stars (NS) are among the densest objects existing in the present universe with a measured and estimated mass in the range of $1-2M_{\odot}$, confined in a sphere of radius ~ 10 km. These tiny but massive stars harbor matter under extreme physical conditions, that remains inaccessible to direct observation. Hence, our knowledge of a NS's interior, including the behavior of matter at such extreme densities, remains theoretical and is the subject of ongoing research and modeling. However, the new generations of telescopes have provided valuable observation data in the recent past and helped refine the theoretical description - called the equation of state (EOS). The EOS of NS plays a critical role in determining various properties of NS, such as their mass, radius, moment of inertia, tidal deformability, oscillation frequencies and the structure of their internal layers. It is essential for understanding the observational characteristics of NS, including their gravitational wave signals, electromagnetic radiation, and thermal emissions. The maximum observed mass of NS $\sim 2M_{\odot}$ ruled out the softer EOS (Cromartie et al. 2019; Fonseca et al. 2021;

Demorest et al. 2010; Antoniadis et al. 2013). The International Space Station (ISS) based X-ray telescope and instrument package, NS Interior Composition Explorer (NICER) measures the mass and radius of a pulsar simultaneously for the first time. Electromagnetic radiation from the hotspots at the magnetic poles of a rotating NS provides us with a direct route of observation when the radiation crosses our line of sight (Miller et al. 2021; Riley et al. 2021). The detection of gravitational waves from NS mergers events have provided stringent limits on tidal deformability for a NS with canonical mass of $1.4M_{\odot}$, adding valuable insights into the EOS (Abbott et al. 2018). The nuclear physics data at the moderate densities combined with recent NICER observations can further improve the constraints. Additionally, new X-ray observatories like the European Space Agency's Athena mission and NASA's Lynx mission are expected to offer even higher-resolution X-ray observations of NS. The third generation Einstein Telescope (ET) (Branchesi et al. 2023) will have a sensitivity ten times better compared to the second generation detectors. Advanced LIGO and Virgo would be optimized for

the detection of gravitational signals at low frequency. Ongoing and future surveys, such as the Square Kilometre Array (SKA), is poised to discover more pulsars and provide a better understanding of the population of NS, their properties. The coordinated observations of NS mergers in multiple wavelengths, such as X-rays, gamma-rays, and radio waves will definitely help advance our understanding of the EOS of dense matter.

The NS core is believed to be made up of neutrons, along with an admixture of protons and leptons. There are several EOS models, that can be broadly categorised into non-relativistic and relativistic models. Among them, the relativistic mean field models (RMF) varieties have been successfully applied to study NS properties as well as finite nuclei properties. Over the decades additional mesons and non-linear self-interaction as well as cross-coupling terms for all the mesons have been added to the original RMF i.e. Walecka Model (Walecka 1974). Various sets of tabulated RMF EOS, compatible with astrophysical observations (Nandi et al. 2019) are available¹ depending upon the on the form of interactions in the Lagrangian density. The associated couplings for the interaction are fitted to various nuclear matter parameters such as binding energy per particle, incompressibility, the symmetry energy coefficients and their derivatives, that are determined from terrestrial experiments at saturation density. Nevertheless the EOS provides a reasonable description of the nuclear matter at suprasaturation densities. The nuclear matter parameters define the NS EOS and are correlated to NS observables (Malik et al. 2023). At this high density, different models consider the possibility of strange matter like hyperons, quarks, Bose-Einstein condensates, under extreme pressures and densities also (Banik et al. 2014; Char et al. 2015; Malik et al. 2021). It's a challenge to unravel the NS core composition and precisely determine its EOS owing our limited knowledge of matter under extreme physical conditions.

In the absence of any universally-acceptable model EOS, subject to limited observational data, several recent works have used the Spectral representations of realistic EOS as an accurate and efficient way of parametrizing the high-density sections of the NS EOS. (Abbott et al. 2018; Miller et al. 2019; Raaijmakers et al. 2020). This is a powerful theoretical tool, to describe the EOS in terms of the spectral functions, incorporating our current knowledge of fundamental physics. The tabulated version of the realistic EOS often infuses numerical error in the calculation of the relevant ther-

modynamic quantities (Servignat et al. 2023). A robust analytic representation of the EOS like the Spectral representation (Lindblom 2010, 2018, 2022), the generalized piecewise polytropic representation (O'Boyle et al. 2020) or the speed of sound parametrization (Tews et al. 2018; Greif et al. 2019) becomes quite useful in scenarios where we need numerical determination of thermodynamic quantities associated with a cold β -equilibrated EOS at any arbitrary energy density inside the NS.

The structure parameters like mass, radius, tidal deformability have taken crucial roles to address the uncertainties in NS EOS. The quasi-periodic oscillations (QPOs) are also valuable tools for studying the compact objects and the processes occurring in their binary systems. NS can exhibit a variety of oscillation modes mainly observed in the X-ray light curves of NS in various types of binary systems, including low-mass X-ray binaries (LMXBs) and NS X-ray binaries. A General Relativistic description of oscillations due to non-radial perturbations involves what are called the quasinormal modes (QNM). Einstein equations govern the dynamics both inside and outside the star. QNMs are different than the normal modes describing Newtonian oscillations of matter inside the star. These modes are damped due to the emission of gravitational waves (GW) from the star. The emitted GWs, given by the perturbations of the spacetime metric tensor, carry information about the internal structure and composition of the NS. The real part of the complex-valued QNM frequency represents the actual frequency of the oscillations, and the imaginary part corresponds to an exponential damping of the wave. Outside the star, the determination of frequency and damping time of the QNMs become an eigenfrequency problem subject to appropriate boundary conditions both at the surface of the NS and at spatial infinity. The internal structure and dynamics of the matter inside it influence the frequencies and damping times of the QNMs via the boundary condition at the surface of the NS. Inside the star, the oscillations of the matter and the GWs are coupled to each other via the Einstein equations.

The study of QNMs of oscillating astrophysical objects started with spherically symmetric black hole spacetimes [See (Regge & Wheeler 1957; Vishveshwara 1970; Zerilli 1970)] and was later extended to compact astrophysical stars (Thorne & Campolattaro 1967) including NS [See the review (Kokkotas & Schmidt 1999) for references]. The modes of oscillation inside the NS are characterized based on the physics behind the restoring force. For example, the pressure of the fluid (which is generally considered incompressible) in the NS interior, acts as the restoring force for p -modes. Buoy-

¹ CompOSE website (<https://compose.obspm.fr>)

ancy restores the so-called gravity g -modes which originates from internal temperature or composition gradients. The most fundamental mode of oscillation is the f -modes which arise out of density perturbations. They typically have a frequency of around 2.4 kHz (Rezzolla 2003; Kokkotas et al. 2001) and have the strongest coupling with the emission of GWs. Determination of the eigen-frequencies while ignoring the metric perturbations during fluid oscillations (relativistic Cowling approximation) to simplify the calculations overestimates the frequency of certain fundamental modes [See the discussion on the accuracy of this approximation in (Sotani & Takiwaki 2020)]. We can improve the accuracy by introducing the emission of GWs and using a post-Newtonian approximation to estimate the damping rate of the f -modes as a result. This way, one can obtain scaling relations between bulk properties of the star, e.g., compactness, mass, moment of inertia and mode frequency, and the damping time (Andersson 2019; Andersson & Kokkotas 1996, 1998; Benhar et al. 2004; Detweiler 1975; Kokkotas et al. 2001). When the problem is treated General Relativistically, we get f -modes for the QNM.

Now, several works in the literature have demonstrated that for f -modes, the relativistic analysis also leads to very similar scaling relations. Such scaling relations can thus be taken as universal [See for example (Andersson & Kokkotas 1996, 1998; Lattimer & Prakash 2001; Yagi & Yunes 2013; Tsui & Leung 2005; Lau et al. 2010)]. This feature of universality can be used as a landmark. One can check how well the calculated frequencies and damping times of the QNMs for a given EOS fit the scaling relations as a sort of consistency requirement [For details, see (Andersson 2021)]. This is a strategy we consistently follow throughout this paper. Another feature of the NS, the tidal deformability, also encodes important information about the shape of the star. An external tidal gravitational field acting on the NS contributes to the quadrupole and higher moments of the matter distribution inside [For more details, see (Andersson & Pnigouras 2020; Pratten et al. 2020; Andersson & Pnigouras 2021; Poisson & Will 2014; Chan et al. 2014)].

Apart from the f -modes, there are also other modes that typically correspond to one or more additional physical processes. These modes mostly have frequencies higher than that of f -modes. For example, the frequency of the g -modes, which appear when the temperature and/or the pressure of the NS vary from one point inside the star to another, can lie in a range starting from the order of 100 kHz (Reisenegger & Goldreich 1992). For this reason, one expects g -modes to appear

when phase transition occurs inside the NS (Andersson 2019). Apart from these, p -modes and r -modes can also occur due to pressure and spin-related instabilities in the NS, respectively [For details, see the review (Andersson 2019) and the references therein]. However, in this work, we focus only on f -modes for the NS, determining their frequencies and damping times from fully general relativistic calculations.

Recent publications (Sotani 2021; Pradhan et al. 2022; Kunjipurayil et al. 2022; Pradhan et al. 2023) show efforts to estimate nuclear matter parameters using stellar oscillation modes. (Pradhan et al. 2022) reported how the effective nucleon mass (m^*) at saturation is correlated with the f -mode frequencies for a set of EOS generated within the relativistic mean field formalism. A strong correlation of the stellar oscillation frequencies with the symmetry energy parameters like $J_{sym,0}$, $K_{sym,0}$, $L_{sym,0}$, and so on would allow us to infer the composition of matter at very high densities in the NS interior (Patra et al. 2023).

In this work we have prepared a set of ~ 9000 nucleonic EOS through Bayesian analysis of relativistic mean field model parameters. We impose constraints of recent interest like the χ EFT and pQCD at relevant energy densities to infer the parameter set. Then we determine a highly accurate Spectral representation of the generated set. We numerically solve the fully General Relativistic perturbation equations for a set of equilibrium configuration NS with varying mass for each EOS. We report the corresponding f -mode frequencies and the gravitational wave damping times over the EOS set. Finally we explore correlation of the frequencies and damping times with nuclear matter parameters and stellar observables.

We organize the paper in the following manner. Sec. 2 provides a brief overview of the relativistic mean field formalism for the nuclear EOS at zero temperature followed by a brief description framework for spectral fitting of the EOS, and the formalism for non-radial quadrupolar oscillations of a non-rotating NS. Sec. 3 contains the results for the set of parametrized spectral version of the entire EOS set. We discuss the results and conclude our work in Sec. 4.

2. FORMALISM

2.1. RMF EOS

We generate a set of EOS within a description of nuclear matter based on a relativistic field theoretical approach where the nuclear interaction between nucleons is introduced through the exchange of the scalar-isoscalar meson σ , the vector-isoscalar meson ω , and the vector-isovector meson ρ . The Lagrangian density is given by

(Dutra et al. 2014; Malik et al. 2023)

$$\mathcal{L} = \mathcal{L}_N + \mathcal{L}_M + \mathcal{L}_{NL} + \mathcal{L}_{leptons} \quad (1)$$

where

$$\mathcal{L}_N = \bar{\Psi} \left[\gamma^\mu \left(i\partial_\mu - g_\omega \omega_\mu - \frac{1}{2} g_\rho \mathbf{t} \cdot \boldsymbol{\rho}_\mu \right) - (m_N - g_\sigma \sigma) \right] \Psi$$

denotes the Dirac equation for the nucleon doublet (neutron and proton) with bare mass m_N , Ψ is a Dirac spinor, γ^μ are the Dirac matrices, and \mathbf{t} is the isospin operator. \mathcal{L}_M represents the mesons, given by

$$\begin{aligned} \mathcal{L}_M = & \frac{1}{2} [\partial_\mu \sigma \partial^\mu \sigma - m_\sigma^2 \sigma^2] - \frac{1}{4} F_{\mu\nu}^{(\omega)} F^{(\omega)\mu\nu} + \frac{1}{2} m_\omega^2 \omega_\mu \omega^\mu \\ & - \frac{1}{4} \mathbf{F}_{\mu\nu}^{(\rho)} \cdot \mathbf{F}^{(\rho)\mu\nu} + \frac{1}{2} m_\rho^2 \boldsymbol{\rho}_\mu \cdot \boldsymbol{\rho}^\mu \end{aligned}$$

where $F^{(\omega,\rho)\mu\nu} = \partial^\mu A^{(\omega,\rho)\nu} - \partial^\nu A^{(\omega,\rho)\mu}$ are the vector meson tensors.

$$\begin{aligned} \mathcal{L}_{NL} = & -\frac{1}{3} b m_N g_\sigma^3 (\sigma)^3 - \frac{1}{4} c (g_\sigma \sigma)^4 + \frac{\xi}{4!} g_\omega^4 (\omega_\mu \omega^\mu)^2 \\ & + \Lambda_\omega g_\rho^2 \boldsymbol{\rho}_\mu \cdot \boldsymbol{\rho}^\mu g_\omega^2 \omega_\mu \omega^\mu \end{aligned}$$

contains the non-linear terms with parameters b , c , ξ , Λ_ω to take care of the high-density behavior of the matter. g_i 's are the couplings of the nucleons to the meson fields $i = \sigma, \omega, \rho$, with masses m_i . Finally, the Lagrangian density for the leptons is given as $\mathcal{L}_{leptons} = \bar{\Psi}_l \left[\gamma^\mu (i\partial_\mu - m_l) \Psi_l \right]$, where Ψ_l ($l = e^-, \mu^-$) denotes the lepton spinor; leptons are considered non-interacting. The equations of motion for the mesons fields are obtained from Euler-Lagrange equations:

$$\sigma = \frac{g_\sigma}{m_{\sigma,\text{eff}}^2} \sum_i \rho_i^s \quad (2)$$

$$\omega = \frac{g_\omega}{m_{\omega,\text{eff}}^2} \sum_i \rho_i \quad (3)$$

$$\boldsymbol{\rho} = \frac{g_\rho}{m_{\rho,\text{eff}}^2} \sum_i t_3 \rho_i, \quad (4)$$

where ρ_i^s and ρ_i are, respectively, the scalar density and the number density of nucleon i . The effect of the non-linear terms on the magnitude of the meson fields is clearly shown through the following terms

$$m_{\sigma,\text{eff}}^2 = m_\sigma^2 + b g_\sigma^3 \sigma + c g_\sigma^4 \sigma^2 \quad (5)$$

$$m_{\omega,\text{eff}}^2 = m_\omega^2 + \frac{\xi}{3!} g_\omega^4 \omega^2 + 2\Lambda_\omega g_\rho^2 g_\omega^2 \rho^2 \quad (6)$$

$$m_{\rho,\text{eff}}^2 = m_\rho^2 + 2\Lambda_\omega g_\omega^2 g_\rho^2 \omega^2, \quad (7)$$

and are solved using the relativistic mean-field approximation with the constraint of β -equilibrium i.e.

$\mu_n - \mu_p = \mu_e$, where μ 's are chemical potential of the respective particles. Also, the total baryon number ($n_p + n_n$) conservation and the charge neutrality condition $n_p = n_e$ are enforced.

The pressure and energy density of the baryons and leptons are given by the following expressions:

$$\begin{aligned} \epsilon = & \sum_{i=n,p,e,\mu} \frac{1}{\pi^2} \int_0^{k_{F_i}} \sqrt{k^2 + m_i^*} k^2 dk \\ & + \frac{1}{2} m_\sigma^2 \sigma^2 + \frac{1}{2} m_\omega^2 \omega^2 + \frac{1}{2} m_\rho^2 \rho^2 \\ & + \frac{b}{3} (g_\sigma \sigma)^3 + \frac{c}{4} (g_\sigma \sigma)^4 + \frac{\xi}{8} (g_\omega \omega)^4 + \Lambda_\omega (g_\rho g_\omega \rho \omega)^2, \end{aligned} \quad (8)$$

where $m_i^* = m_i - g_\sigma \sigma$ for protons and neutrons and $m_i^* = m_i$ for electrons and muons, and k_{F_i} is the Fermi moment of particle i . The pressure is determined from the thermodynamic relation, in which every component we could derive out

$$p = \sum_i \mu_i \rho_i - \epsilon. \quad (9)$$

Once we have an EOS model, we can determine various nuclear saturation properties, which are represented by expansion coefficients around the saturation density of both symmetric and asymmetric nuclear matter (Agrawal et al. 2021). We generate our set of EOS using Bayesian inference with minimal constraints. These constraints include nuclear saturation properties such as a saturation density of $\rho_0 = 0.153 \pm 0.005 \text{ fm}^{-3}$, a binding energy of $e_0 = -16.1 \pm 0.2 \text{ MeV}$, nuclear incompressibility of $K_0 = 230 \pm 40 \text{ MeV}$, and a symmetry energy of $J_0 = 32.5 \pm 1.8 \text{ MeV}$ at the saturation density. Furthermore, a low density constraint for the pure neutron matter pressure from chiral effective field theory (χ EFT) (Hebeler et al. 2010) with twice the uncertainty and the NS mass corresponding to the EOS is above the observed $2M_\odot$ was applied. Additionally, the perturbative Quantum Chromodynamics (pQCD) derived constraint at eight times the baryon density ($n_s = 0.16 \text{ fm}^{-3}$) for a pQCD scale $X = 4$ (Komoltsev & Kurkela 2022). Finally, we chose $\sim 9,000$ nucleonic EOS for the present calculation.

2.2. Spectral representation of EOS

We find the spectral parameters for our set of EOS by fitting the tabular RMF EOS with a spectral version. We follow the methodology in (Lindblom 2010) to find faithful representations of realistic EOS for nuclear matter inside the NS by constructing spectral expansions of key thermodynamic quantities. Linear combinations of a complete set of functions like the Fourier basis functions allow us to expand a thermodynamic quantity like

the adiabatic index, defined as

$$\Gamma(p) = \frac{\epsilon + p}{p} \frac{dp}{d\epsilon}. \quad (10)$$

The coefficients of such basis functions in the expansion uniquely determine any given physically valid EOS. One can find that such a representation satisfies the basic necessary thermodynamic conditions. To obtain a pressure-based form, we expand the adiabatic index $\Gamma(p)$ in terms of the basis functions $\Phi_k(p)$ as

$$\Gamma(p) = \exp \left[\sum_k \gamma_k \Phi_k(p) \right]. \quad (11)$$

We choose $\Phi_k(p) = \Phi_k(x)$, where x is a dimensionless logarithmic pressure variable $x = \log(p/p_0)$ as in (Lindblom 2010), p_0 being the minimum pressure where the high-density part of the EOS is joined to the low-density part of BPS(Baym et al. 1971) EOS. The γ_k 's are the spectral coefficients. Numerical integration of the following gives us the EOS $\epsilon(p)$ for the obtained expansion of $\Gamma(p)$

$$\epsilon(p) = \frac{\epsilon_0}{\mu(p)} + \frac{1}{\mu(p)} \int_{p_0}^p \frac{\mu(p')}{\Gamma(p')} dp', \quad (12)$$

where $\mu(p)$ is the chemical potential defined as

$$\mu(p) = \exp \left[- \int_{p_0}^p \frac{dp'}{p' \Gamma(p')} \right]. \quad (13)$$

The energy density at the minimum pressure p_0 is the constant of integration ϵ_0 . The low-density EOS is matched at this pressure slightly below the nuclear saturation density such that there is no unexpected phase transition at the junction. One can determine an empirical fit to any given EOS with arbitrary accuracy by increasing the number of basis functions used. We have 4 spectral coefficients corresponding to four basis functions as in (Lindblom 2010) for fitting the set of RMF EOS we are using. We plot distribution of the spectral parameters $\gamma_0, \gamma_1, \gamma_2, \gamma_3, p_0$ in Fig. 2. Apart from the coefficients, parameters ϵ_0 and x_{max} have fixed values. We do optimization of the spectral coefficients, γ_k , by minimizing the differences between $\epsilon_{fit}(x_i, \gamma_k)$ and the energy density $\epsilon_i = \epsilon(x_i)$ values from the tabular version of EOS for a specific set of x 's (or p 's). The following residue quantifies the faithfulness of the fitting

$$\Delta^2(\gamma_k) = \sum_{i=1}^N \frac{1}{N} \left\{ \log \left[\frac{\epsilon_{fit}(x_i, \gamma_k)}{\epsilon_i} \right] \right\}^2 \quad (14)$$

where we sum over the chosen pressure values between $p_0 \leq p_i \leq p_{max}$; p_{max} is the pressure at the center of the

non-rotating maximum mass NS for the given EOS. The spectral version of the EOS serves as the input for the Tolman-Oppenheimer-Volkoff equations, which gives us the equilibrium configuration of the star.

2.3. Metric with perturbations

To determine the frequencies of the f-modes, we solve the Einstein equations $G_{\mu\nu} = 8\pi GT_{\mu\nu}$. We assume here that the gravitational waves are perturbations of the static background spacetime metric for the non-rotating NS. The perturbed metric has the form:

$$g_{\mu\nu} = g_{\mu\nu}^0 + h_{\mu\nu}, \quad (15)$$

The time dependence of the perturbed metric components can be expressed by the factor $e^{i\omega t}$ for a wave mode. Here ω is complex as the waves will decay due to the imposed open boundary conditions, which will be discussed shortly. The real part of ω is the frequency, while the imaginary part gives the inverse of the damping time (if it is positive) of the wave mode. These oscillations are studied considering the linearized Einstein equations, coupled with the equations of hydrodynamics, for our set of EOS, with suitably posed boundary conditions. A small perturbation $h_{\mu\nu}$ is assumed on a static spherically symmetric background metric given by

$$\begin{aligned} ds^2 = & -e^{\nu(r)} [1 + r^l H_0(r) e^{i\omega t} Y_{lm}(\phi, \theta)] c^2 dt^2 \\ & + e^{\lambda(r)} [1 - r^l H_0(r) e^{i\omega t} Y_{lm}(\phi, \theta)] dr^2 \\ & + [1 - r^l K(r) e^{i\omega t} Y_{lm}(\phi, \theta)] r^2 d\omega^2 \\ & - 2i\omega r^{l+1} H_1(r) e^{i\omega t} Y_{lm}(\phi, \theta) dt dr, \end{aligned} \quad (16)$$

Here $e^{\lambda(r)} = \frac{1}{1 - \frac{2Gm(r)}{c^2 r}}$ and $e^{\nu(r)} = \exp \left(\frac{2G}{c^2} \int_0^r \left\{ \frac{m(r') + \frac{4\pi p(r') r'^3}{c^2}}{r' \left[r' - \frac{2m(r')G}{c^2} \right]} \right\} dr' \right) e^{\nu_0}$; $m(r')$ and $p(r')$ being the enclosed mass and pressure of the star at r' . Here $H_0, H_1,$ and K are radial perturbations of the metric and the angular part is contained in the spherical harmonics Y_m^l with l denoting the orbital angular momentum number and m the azimuthal number.

2.4. Lindblom-Detweiler equations

The perturbations of the energy-momentum tensor of the fluid also need to be taken into account in the Einstein equation. The components of Lagrangian displacement vector $\xi^a(r, \theta, \phi)$ describes the perturbations of the fluid inside the star:

$$\xi^r = r^{l-1} e^{-\lambda/2} W Y_m^l e^{i\omega t} \quad (17)$$

$$\xi^\theta = -r^{l-2} V \partial_\theta Y_m^l e^{i\omega t} \quad (18)$$

$$\xi^\phi = -\frac{r^{l-2}}{\sin^2 \theta} V \partial_\theta Y_m^l e^{i\omega t}, \quad (19)$$

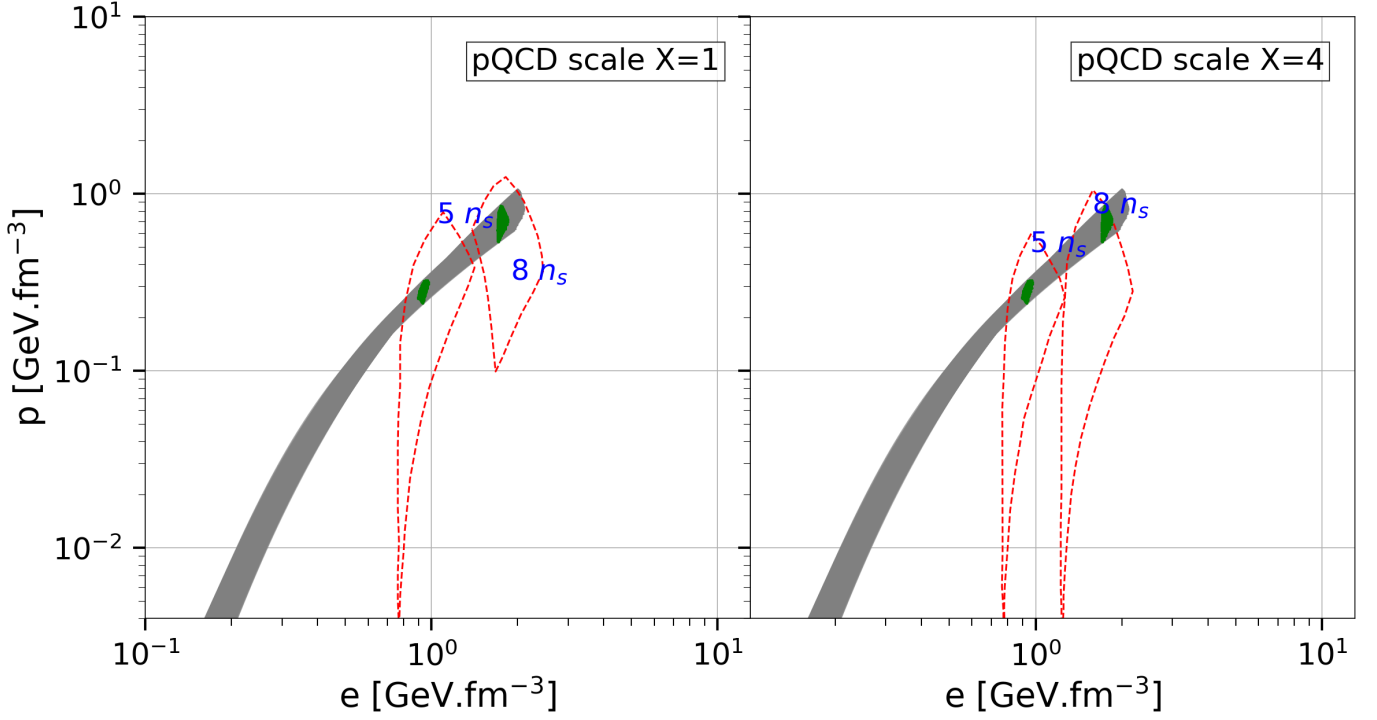


Figure 1. We display the pressure and energy density for the selected EOS set, enclosing areas compliant with pQCD-derived restrictions for baryon number densities equal to $5n_s$ and $8n_s$ (where $n_s=0.16 \text{ fm}^{-3}$) (Komoltsev & Kurkela 2022) by red dashed lines, informed by the stringent renormalization scale parameter, $X = 1$ ($X = 4$), according to (Kurkela et al. 2010) in the left panel (right panel). We indicate the energy densities and pressures that satisfy the pQCD constraints by green patches for the corresponding number densities. It will be significant to note that the central density for the maximum mass NS is modeled within $7n_s$ across our entire EOS set.

where W and V are functions with respect to r that describe fluid perturbations. Fluid perturbations exist only inside the star. The introduction of a new variable X leads to simplification of perturbation equations for NS interior. X is related to the rest of the perturbation functions through the following equations

$$H_0 = \left\{ 8\pi r^2 e^{-\nu/2} X - [(n+1)Q] - \omega^2 r^2 e^{-(\nu+\lambda)} H_1 + [n - \omega^2 r^2 e^{-\nu} - e^\lambda Q(Q - e^{-\lambda})] K \right\} (2b + n + Q)^{-1}, \quad (20)$$

$$V = \left[\frac{X}{\epsilon + p} - \frac{Q}{r^2} e^{(\nu+\lambda)/2} W - e^{\nu/2} \frac{H_0}{2} \right] \frac{e^{\nu/2}}{\omega^2}, \quad (21)$$

where $n = (l-1)(l+2)/2$, $b = Gm/rc^2$, $Q = b + 4\pi Gr^2 p/c^4$, and ϵ is the local energy density. The gravitational wave equations can be written as a set of four coupled linear differential equations for the four perturbation functions: H_1 , K , W , and X , which do not diverge inside the star for any given value of ω (Lindblom & Detweiler 1983).

$$r \frac{dH_1}{dr} = -[l+1 + 2be^\lambda 4\pi r^2 e^\lambda (p - \epsilon)] H_1 + e^\lambda [H_0 + K - 16\pi(\epsilon + p)V], \quad (22)$$

$$r \frac{dK}{dr} = H_0 + (n+1)H_1 + [e^\lambda Q - l - 1] K - 8\pi(\epsilon + p)e^{(\lambda/2)} W, \quad (23)$$

$$r \frac{dW}{dr} = -(l+1) [W + le^{\lambda/2} V] + r^2 e^{\lambda/2} \left[\frac{e^{-\nu/2} X}{(\epsilon + p)c_{eq}^2} + \frac{H_0}{2} + K \right],$$

$$r \frac{dX}{dr} = -lX + \frac{(\epsilon + p)e^{(\nu/2)}}{2} \left\{ (3e^\lambda Q - 1)K - \frac{4(n+1)e^\lambda Q}{r^2} V + (1 - e^\lambda Q)H_0 + (r^2 \omega^2 e^{-\nu} + n + 1)H_1 - \left[8\pi(\epsilon + p)e^{\lambda/2} + 2\omega^2 e^{\lambda/2 - \nu} r^2 \times \frac{d}{dr} \left(\frac{e^{-\lambda/2}}{r^2} \frac{d\nu}{dr} \right) \right] W \right\}. \quad (24)$$

where $c_{eq}^2 = dp/d\epsilon$ is the equilibrium speed of sound of NS matter undergoing oscillations.

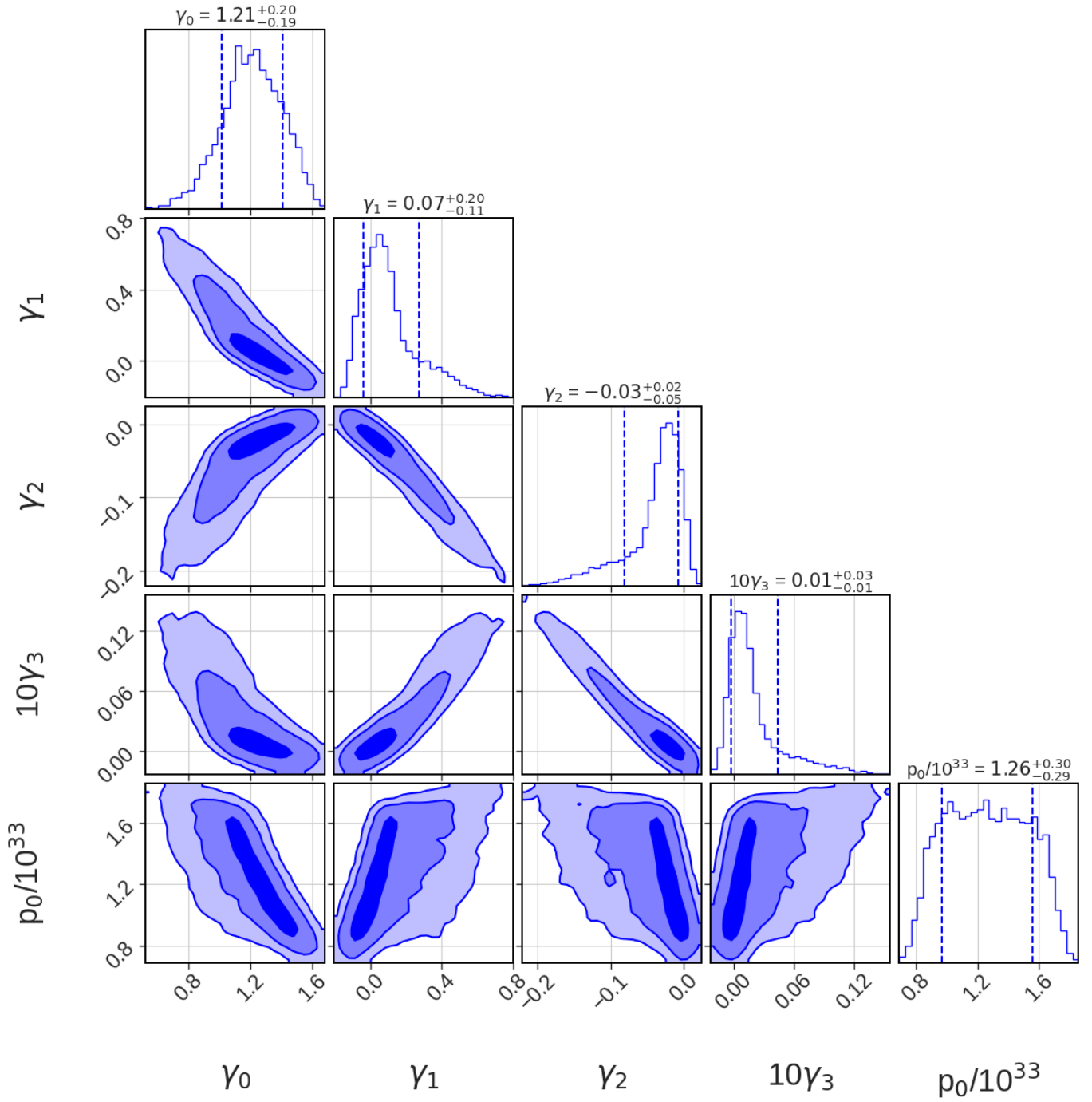


Figure 2. The corner plot shows the distributions of parameters γ_0 , γ_1 , γ_2 , γ_3 , and p_0 from the spectral representation of the EOS within the acquired set of RMF EOS for this study. Vertical lines indicate the 90% credible intervals (CIs), while varying shades in the 2D distribution denote the 1σ , 2σ , and 3σ CIs, respectively.

2.5. Boundary conditions for perturbation equations

We discuss the boundary conditions imposed here to solve the Einstein equations inside the star. For that, one needs to integrate the perturbation equations from the center of the star to a certain radius inside the star. The boundary condition for the perturbation functions at the center of the star $r = 0$ are

$$\begin{aligned} W(0) &= 1, \\ X(0) &= (\epsilon_0 + p_0)e^{\nu_0/2} \\ &\left\{ \left[\frac{4\pi}{3}(\epsilon_0 + 3p_0) - \frac{\omega^2}{l}e^{-\nu_0} \right] W(0) + \frac{K(0)}{2} \right\}, \\ H_1(0) &= \frac{lK(0) + 8\pi(\epsilon_0 + p_0)W(0)}{n + 1}, \end{aligned} \quad (25)$$

The condition $\Delta p = 0$ at $r = R$, the star's surface, requires the perturbation function X to be equal to zero at the surface of the star. We assign some small arbitrary values to the functions H_1 , K , and W at the star's surface and integrate backward to reach the point at which the integration from the center of the star ends and join the two forward and backward solutions. To find the quasinormal mode frequency for a given star, we solve the Zerilli equation outside the star using the method of continued fraction developed by Leins, Nollert, and Soffel (Leins et al. 1993) as done in (Sotani et al. 2001) ensuring that the wave is outgoing far away from the star. This is sometimes referred to as the *open boundary condition* for the gravitational waves.

3. RESULTS

Our primary aim is to comprehensively examine the f -mode oscillations, one of the non-radial oscillatory modes of NS over a broad range of realistic EOS. To achieve this, we employ the linearized full General Relativity approach. For this work, we prepare a set of realistic nuclear EOS that only have nucleonic composition, obtained with the relativistic mean-field (RMF) approach. We utilize around 9,000 nucleonic EOS that were acquired through Bayesian Inference with minimal restrictions imposed on them, as previously mentioned in Sec. 2.1. The range of nuclear saturation properties, including the binding energy e_0 , nuclear incompressibility K_0 , skewness parameter Q_0 , symmetry energy $J_{\text{sym},0}$, its slope $L_{\text{sym},0}$ and its curvature $K_{\text{sym},0}$ at the saturation density n_0 , is presented in Table 1. Our tabulated set of EOS is given a functional representation by spectral Decomposition Method (see Sec. 2.2). This is a reliable approach which is often used in the context of NS interior structure calculations. Using a minimal

number of spectral coefficients, we achieved a fit of all our $\sim 9\text{K}$ EOS with a precision of less than 0.5% using the Levenberg-Marquardt method for optimization of the residual error in Eq. 14 as done in (Lindblom 2010, 2018).

In Fig. 1, we plot the entire EOS set employed in this work and compare with constraints derived from perturbative Quantum Chromodynamics (pQCD) at baryon densities of $5n_s$ and $8n_s$, with $n_s = 0.16 \text{ fm}^{-3}$. The plot is divided into two panels, representing two different renormalization scales, ($X = 1$) and ($X = 4$), for the pQCD constraints. The left panel focuses on the renormalization scale ($X = 1$) of the pQCD constraints, with the green patch indicating the energy densities and pressure points for each EOS at the respective baryon densities that are in agreement with the pQCD constraints. All the EOS in our set meet the requirements set by pQCD results up to $8n_s$ and a renormalization scale of 4. However, the central density for maximum-mass NS for all the EOS in our set is below $7n_s$.

In Fig. 2, we present a corner plot showing the distribution of the spectral parameters for our set of $\sim 9\text{K}$ RMF EOS. This visual representation is essential to understand the statistical properties and correlations among the parameters. The diagonal plots contain representations of the marginalized 1D distribution of individual parameters, while the off-diagonal plots illustrate the 2D distribution for pairs of parameters, giving insight into their mutual relationships. The value of median of each spectral parameter along with error bars are labeled on the respective diagonal plots, here the dashed vertical lines mark the limits of the errors. The color gradient, which changes from dark to light blue in the 2D graphs, symbolizes the confidence intervals: 1σ , 2σ , and 3σ . The elliptical shapes observed in the 2D plots indicate strong correlations among the parameters. If the shape approaches a circle, it signifies a weak correlation between the given parameter pair. An interesting observation from the figure is that most of the γ_i parameters show strong correlations with their subsequent γ_{i+1} parameters. This trend is expected; to ensure a smooth EOS an increase in a particular γ must be related to the previous one. This aspect of parameter correlation is essential for maintaining a coherent and smooth representation of the EOS, thus confirming the effectiveness of the spectral decomposition format in capturing the essential characteristics of the dense matter EOS.

In Fig. 3, we plot the mass-radius (MR) of the NS (left) and the mass-tidal deformability (right) of all EOS considered using the spectral representation of the EOS (see Sec. 2.1). The gray zones in the left panel represent the 90% (dark) and 50% (light) confidence intervals

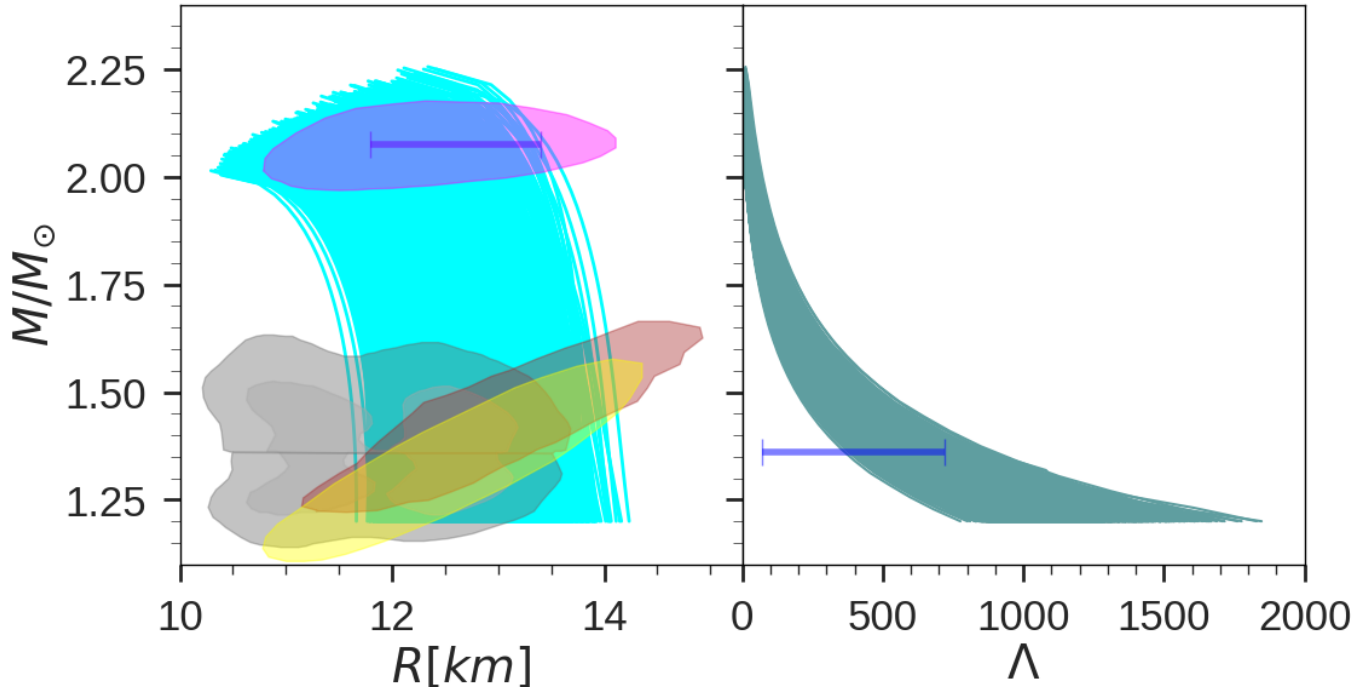


Figure 3. The NS mass-radius and mass-tidal deformability curves are plotted for the entire set of EOS used in this work. The gray zones in the left panel indicate 90%(dark) and 50%(light) confidence intervals for the binary components of the GW170817 event (Abbott et al. 2018). The brown and yellow zones in the same panel represent the credible zone 1σ (68%) of the 2-D posterior distribution in the mass-radius domain of millisecond pulsar PSR J0030+0451 in (Riley et al. 2019) and (Miller et al. 2019) respectively, while the magenta zone is for PSR J0740+6620 (Riley et al. 2021; Miller et al. 2021) based on the NICER X-ray data. The blue bars represent the radius of PSR J0740+6620 at $2.08M_{\odot}$ (left panel) and its tidal deformability at $1.36M_{\odot}$ (right panel) (Abbott et al. 2018).

Table 1. Nuclear matter parameters calculated at saturation density for the 9K EOS used in this work, along with the median and 90% confidence interval.

Model	e_0 (MeV)	n_0 (fm^{-3})	K_0 (MeV)	Q_0 (MeV)	$J_{sym,0}$ (MeV)	$L_{sym,0}$ (MeV)	$K_{sym,0}$ (MeV)	m^*
NL	$-16.10^{+0.33}_{-0.33}$	$0.152^{+0.008}_{-0.005}$	255^{+42}_{-40}	-451^{+154}_{-71}	$32.07^{+2.52}_{-2.77}$	32^{+13}_{-21}	-96^{+96}_{-54}	$0.74^{+0.03}_{-0.10}$

for the binary components of the GW170817 event (Abbott et al. 2019). The predictions of NS radius measurements from NICER X-ray data for the PSR J0030+0451 and PSR J0740+6620 pulsars are also included, with the 1σ (68%) confidence zone of the 2-D posterior distribution in the MR domain of the millisecond pulsar PSR J0030+0451 shown in brown and yellow from references (Riley et al. 2019) and (Miller et al. 2019) respectively, and PSR J0740+6620 in magenta (Riley et al. 2021; Miller et al. 2021). Finally, the blue bars represent the tidal deformability of PSR J0740+6620 at $2.08M_{\odot}$ and $1.36M_{\odot}$ (right panel) (Abbott et al. 2018). All MR curves have a maximum mass greater than $2M_{\odot}$, since this was imposed while Bayesian sampling. Despite the lack of constraints on radius and tidal deformability during sampling, the prediction of NS mass and radius is

still able to meet the entire EOS set with the minimal requirements that were set. The obtained radius of a $1.4M_{\odot}$ NS in our set is 12.03-13.20 km, and the deformability of the tidal channel for a $1.36M_{\odot}$ star is 431 – 659 within 90% confidence interval. The maximum mass of a NS ranges from 2 to $2.25M_{\odot}$, which is consistent with the results reported in Rezzolla et al. (2018). It is worth noting that we applied perturbative Quantum Chromodynamics (pQCD) constraints to our EOS set, which limited the maximum mass of a NS to a certain range and eliminated some of the stiffer EOS.

We display the f -mode frequencies in Fig. 4 (left) versus NS mass. It increases from 1.6 to 2.6 kHz for variation of NS mass from 1.2 to $2.25M_{\odot}$ forming a band of frequencies that spans from 0.3 to 0.4 kHz as the mass increases. It is worth noting that, the f -mode frequency

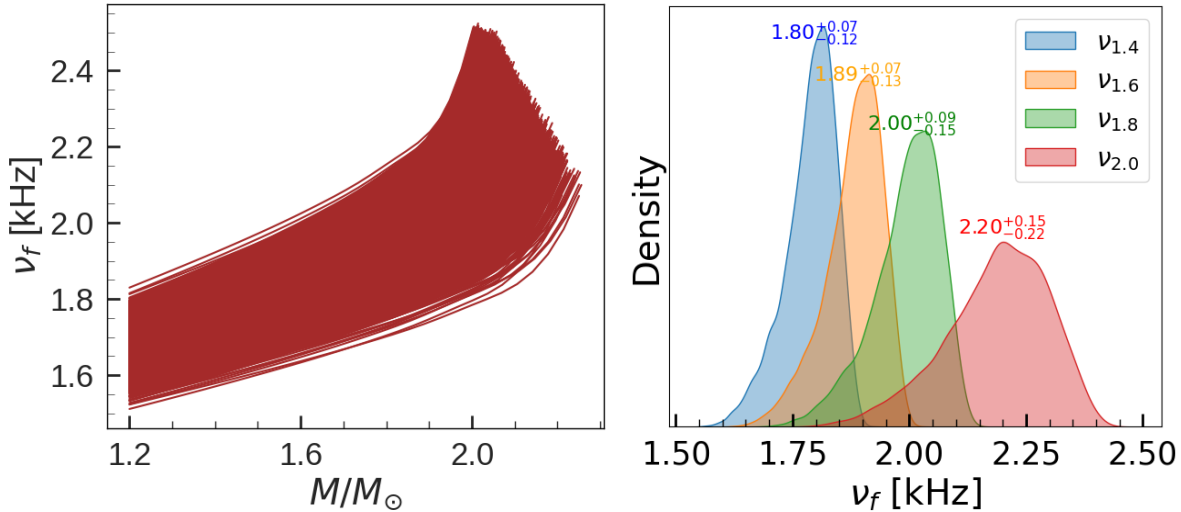


Figure 4. The frequency of the f -mode oscillations, calculated using linearized GR, is shown on the left for the EOS set utilized. On the right, the density distribution of the f -mode frequency for different NS masses in the range of $1.4M_\odot$ to $2.0M_\odot$ is plotted.

within the Cowling approximation for NSs with a mass greater than $2M_\odot$ is in the range of 2.1 - 2.7 kHz and 2.3 - 2.65 kHz for the two types of EOS used in (Kumar et al. 2023), respectively. It is a widely accepted fact that the calculation of the f -mode frequencies using the Cowling approximation, overestimates them by up to 30 to 10 percent for NS with masses ranging from 1.0 to $2.5 M_\odot$, when compared to the frequency obtained from the linearized general relativistic formalism Benhar et al. (2004); Doneva et al. (2013); Pradhan et al. (2022). In the right panel, we plot the distribution of f -mode frequencies for different NS mass ranging from 1.4 to $2.0 M_\odot$, each distribution is accompanied by its median value and a 90% confidence interval (CI). This variation in the f -mode frequencies across various NS masses is indicative of the current understanding of the EOS for NS. The measurements of f -mode frequencies (with precision beyond the current uncertainty of approximately 0.2 kHz) by the next generation detectors could potentially lead to a more constrained and refined understanding of the EOS domain for the NS interior.

Next we calculate the gravitational wave damping times corresponding to the f -mode frequencies for our EOS set. The inverse of the imaginary part of ω in the metric perturbations gives us the damping time as discussed in Sec.3. In Fig. 5 we plot the variation of damping times with stellar mass. We obtain a monotonically decreasing trend for the damping times with increase in NS mass for all the EOS. The damping time of a $1.4M_\odot$ NS is above 0.1 s and it falls much below 0.1 s for NS with mass above $2M_\odot$. The range of damping times in this work, is slightly below the range(0.13

- 0.51s) of (Pradhan et al. 2022) for their set of RMF EOS.

In the following, we explore the linear dependence between various spectral parameters, nuclear saturation properties, the pressure of NS matter at two and three times saturation density, and other NS properties. We will also examine how the frequency of the f -mode oscillation for different masses relates to the individual components of our nuclear EOS set. We calculate the Pearson correlation coefficients between these quantities using the entire $\sim 9K$ EOS set. The heatmap's

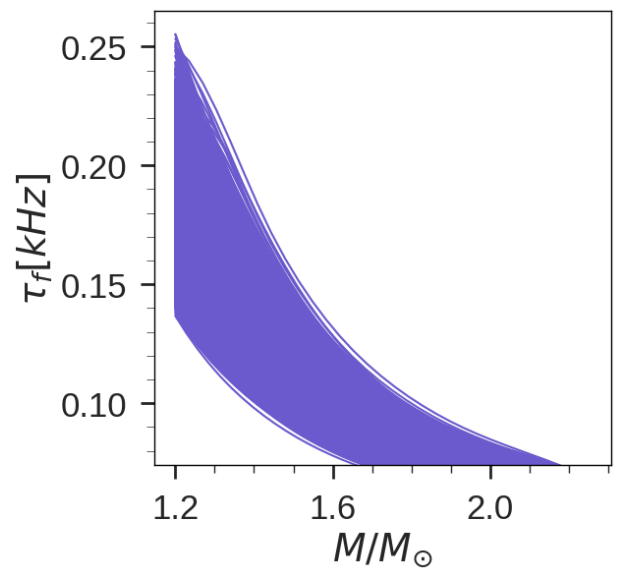


Figure 5. Plot of the gravitational wave damping time, τ_f for the corresponding f -mode oscillation as a function of stellar mass for the 9K RMF EOS set used in this work.

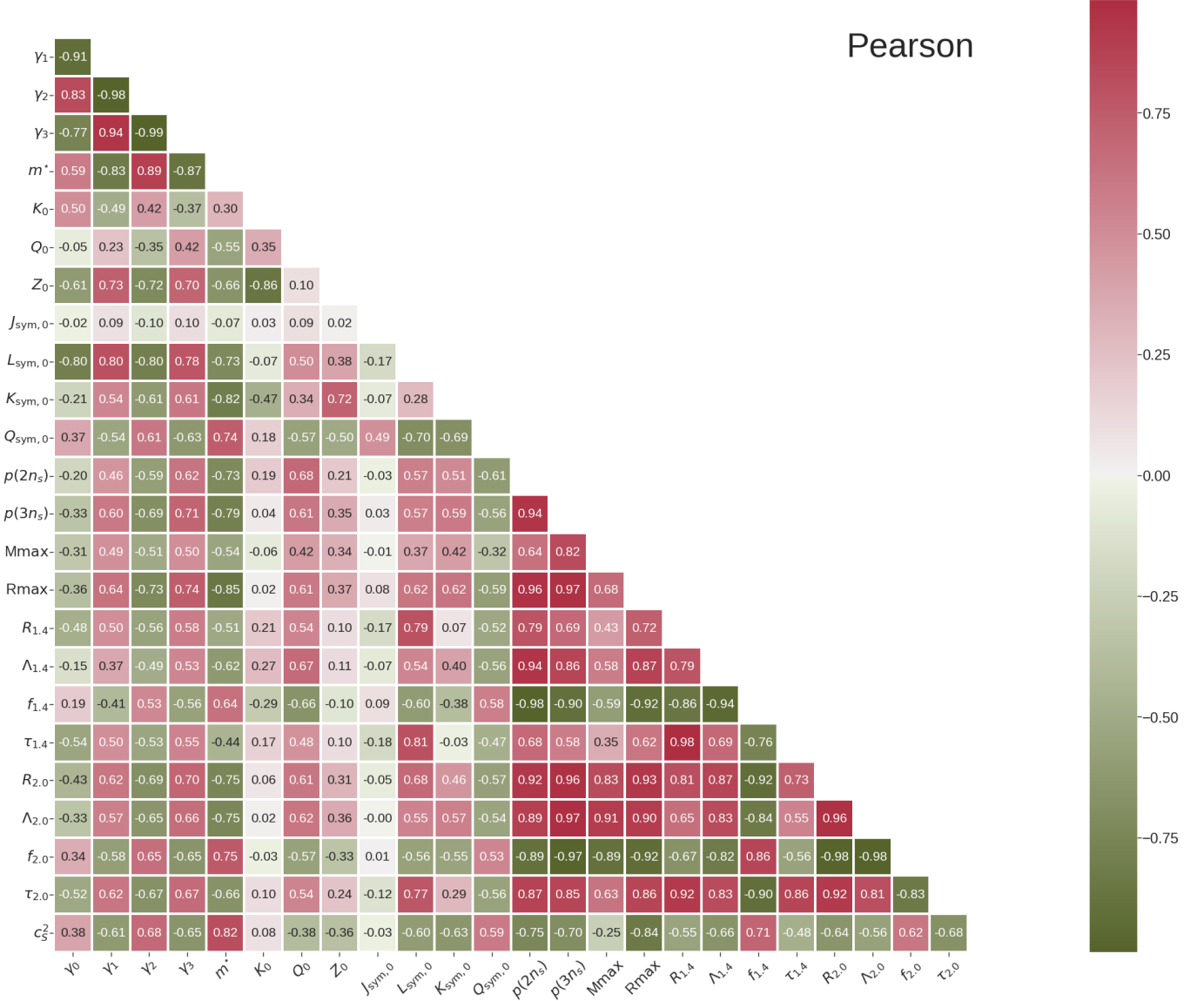


Figure 6. Heatmap displaying the Pearson correlation coefficients among the spectral parameters ($\gamma_0, \gamma_1, \gamma_2, \gamma_3$), nuclear matter parameters (m^*, K_0, Q_0 , etc.), pressure at multiples of saturation number density $n_s = 0.16 \text{ fm}^{-3}$, and stellar observables like mass, radius, f -mode frequency, etc. Subscripts with the corresponding NS property stand for the NS mass associated with that property.

color spectrum, ranging from green to red, indicates the strength of the correlation, from negative to positive, respectively. A deeper red hue indicates a stronger positive correlation, with coefficients above 0.8 indicating a particularly strong linear relationship. The correlation between the spectral parameters γ_1, γ_2 and γ_3 is exceptionally high, clearly indicating a linear relationship between them. This is also true for the pair m^* and the γ_i , suggesting that the effective mass of the nucleon has a strong influence on these spectral parameters. Another finding is the strong correlation, greater than 0.9, between $P(2n_s)$ and $P(3n_s)$, which are the pressures β at twice and three times the saturation density of nu-

clear matter and various properties of NS such as radius, deformability of the tidal, frequency of the mode f and damping time for NS masses of 1.4 and 2.0 M_\odot . This suggests a considerable degree of linear dependence between the properties of NSs of different masses and the overall EOS, rather than individual nuclear saturation properties. The results of previous research are consistent with our current findings. It is worth emphasizing the strong correlation previously reported in Ref. Pradhan et al. (2022) between the fundamental f -mode frequency of different NS masses and the nucleon effective mass at saturation m^* , appears to be less pronounced in our study using the chosen set of EOS. This diver-

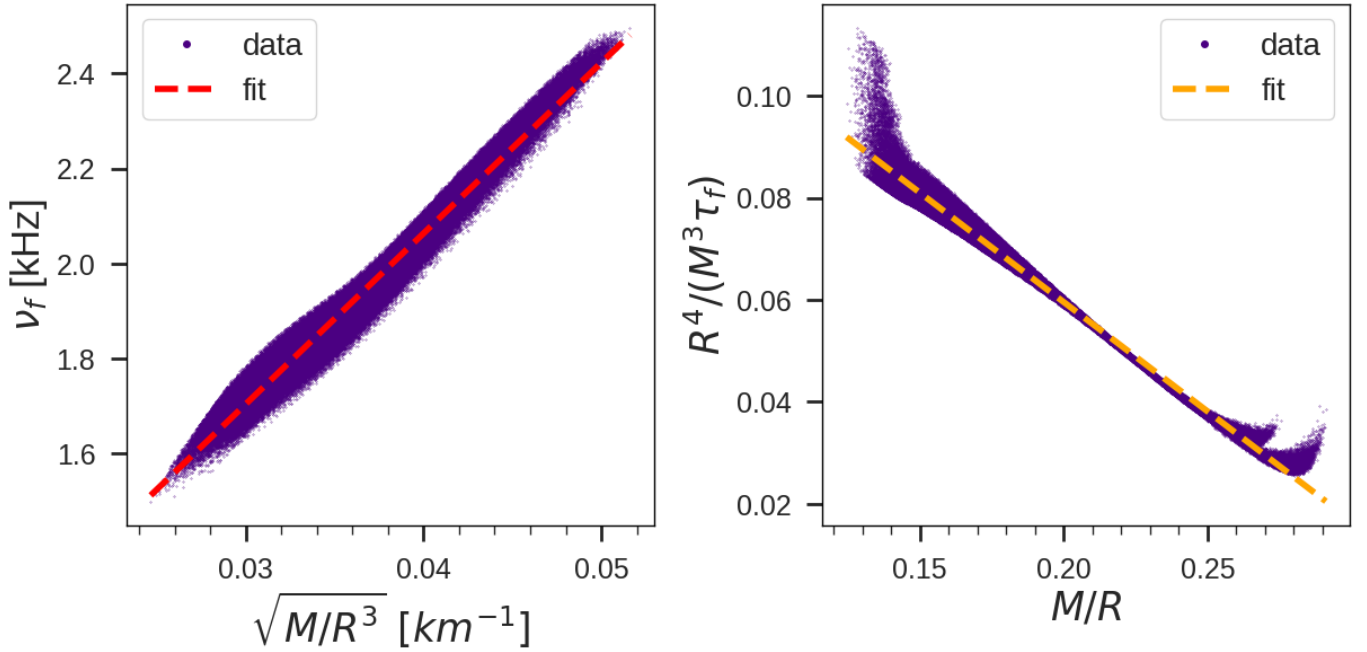


Figure 7. Empirical relation between the f -mode frequency with the average stellar density (left panel) and that between the corresponding dimensionless gravitational wave damping time and the stellar compactness for the set of 9K RMF EOS used in this work. Stellar mass M , radius R , and damping time τ_f are in km.

gence can be mainly attributed to some differences in the EOS that were taken into account. The EOS set employed in our research was generated through Bayesian inference subject to constraints. Specifically, for our low density pure neutron matter EOS, constraints from chiral effective field theory (χ EFT) and perturbative quantum chromodynamics (pQCD) were included 8 times the saturation density n_s (where $n_s = 0.16 \text{ fm}^{-3}$) were included. These constraints were not considered by the other authors. An additional notable distinction is the inclusion of an interaction ω^4 in the Lagrangian that we studied. It is important to note that this term ω^4 tends to soften the EOS, which is a characteristic favored by pQCD analysis. The heatmap suggests that the maximum radius of a NS is closely related to its $R_{1.4}$, $R_{2.0}$, and $f_{2.0}$ values. Furthermore, the f -mode frequencies of NS with 1.4 , and $2.0M_\odot$, namely $f_{1.4}$, and $f_{2.0}$, are strongly correlated with their tidal deformabilities $\Lambda_{1.4}$, and $\Lambda_{2.0}$, respectively, providing insight into how the internal structure of NS responds to tidal forces.

Asteroseismology, the study of stellar oscillations, allows us to infer global NS properties such as mass, radius, and average stellar density from f -mode frequencies and the gravitational wave damping time through certain empirical relations. We describe the results for some selected relations in the following paragraphs.

In Fig. 7 we plot the data with the straight line fit using:

$$\nu_f = a\sqrt{M/R^3} + b \quad (26)$$

This empirical relation is well-known since the publication of (Andersson & Kokkotas 1998). We find the slope a to be $35.94 \pm 0.0113 \text{ kHz.km}$ and the intercept b to be $0.6260 \pm 0.0004 \text{ kHz}$. We can compare these values with the values reported in (Pradhan et al. 2022) (See Table 2). They calculated the f -mode frequencies with a different set of RMF EOS and found the slope equal to 36.20 kHz.km and the intercept equal to 0.535 kHz . The reference in (Kumar et al. 2023) report the same coefficients with values: $a = 22.27, 26.76$ and $b = 1.520, 1.348$ corresponding to determination of f -modes with Cowling approximation for a set of hybrid and a set of purely nucleonic EOS with density dependent couplings. The values for a and b thus appears to be dependent on the set of EOS considered and makes the empirical Eq. 26 somewhat EOS dependent. The relative percentage error for the aforementioned fit in this work is 2.84%.

We display another empirical relation:

$$\frac{R^4}{M^3\tau_f} = a\frac{M}{R} + b, \quad (27)$$

in the right panel of Fig. 7. τ_f is the gravitational wave damping time, equal to the inverse of the imaginary part of ω . (Andersson & Kokkotas 1998) mentioned the existence of this scaling between a dimensionless damping

Empirical relation	Fitting function	Coefficients of current work	Relative error	Coefficients of (Pradhan et al. 2022)	Coefficients of (Kumar et al. 2023)
$f - \sqrt{M/R^3}$	$ax + b$	$a = 35.94 \pm 0.0113$ $b = 0.6260 \pm 0.0004$	2.84%	$a = 36.20$ $b = 0.535$	$a = 22.27, 26.76$ $b = 1.520, 1.348$

Table 2. Coefficients of the fitting equation for the empirical relations Eq.26

time and the compactness for the first time. Both the coefficients a and b are dimensionless and we find the following values (See Table 3): $a = -0.4286 \pm 0.0001$, $b = 0.1453 \pm 2.0 \times 10^{-5}$ with a relative error of 0.19%. (Pradhan et al. 2022) reported the values: $a = -0.245$ and $b = 0.080$. These empirical relations have poor validity beyond $M/R > 0.25$ (Tsui & Leung 2005).

(Kumar et al. 2023) have reported a new scaling between the f -mode frequency and the radius for a NS of given stellar mass:

$$f_x = aR_x + b, \quad (28)$$

where x is the mass of the NS in M_\odot units. We plot the relation with our results of f -mode frequencies for $1.4M_\odot$ and $2.0M_\odot$ in Fig. 8. We find the values (See Table 4): $a = -0.1202 \pm 0.0007$, $b = 3.307 \pm 0.0096$ for $1.4M_\odot$ and $a = -0.2367 \pm 0.0004$, $b = 4.948 \pm 0.0057$ for $2.0M_\odot$. The maximum relative errors are 2.56% and 2.22% respectively. The slope reported in (Kumar et al. 2023) for masses over the range $1.6M_\odot - 2.4M_\odot$ is around -0.22 and the intercept is around 5.1 with 1.5% relative error. A general relativistic treatment of the stellar oscillations in this work presents us with two different slopes for the two cases. This difference is due to the overestimation of f -mode frequencies that occurs when one employs Cowling approximation, as done in (Kumar et al. 2023). From a specific observed value of f -mode frequency for $1.4M_\odot$, we can infer a lesser value of radius from the fit in this work as compared to the fit in (Kumar et al. 2023).

In the study inspired by Lin & Steiner (2023), we delve into the relationship between the radii of NS with masses of $1.34M_\odot$ and $2.0M_\odot$, utilizing our database of 9K nucleonic EOS. Our analysis, shown in Figure 9, presents two key findings.

We show a scatter plot of the radii of NS with masses of $1.34M_\odot$ and $2.0M_\odot$ on the left. This shows a strong correlation, with a Pearson’s correlation coefficient of approximately 0.9, for the 9K nucleonic EOS set utilized. The left blue patch, marked with dashes, represents the constraints derived from NICER observations of PSR J0740+6620 and PSR 0030+0451. NICER’s 1σ posterior distributions were used to obtain these constraints while accounting for a correlation of about 0.9 between the radius of $1.34M_\odot$ and $2.0M_\odot$ NS masses. This method was based on data reported in (Riley et al.

2019, 2021). To be more specific, we produced 1000 random samples of $R_{1.34}$ and $R_{2.07}$ within the 1σ range of the NICER’s observed values over marginalized on NS masses and implemented a correlation of approximately 0.9 between the two radii.

The plot shows a noticeable difference in the slope of the data points between the entire nucleonic EOS and those derived from the NICER observations. In the left panel, represented with a red dashed outline, the most probable region (approximately within 1 standard deviation or ($\sim 1\sigma$)) is represented from the joint posterior distribution calculated in the study by Lin et al. (2023). The data set being discussed fully overlaps with this most probable region. Despite their conclusion that 48% identification probability (with a 5% false alarm rate) that the NICER observations indicate the necessity for a sharp and strong phase transition, the current data set in our calculation shows that even a purely nucleonic composition fits well within this region. The implications of the strong correlation between the radii and the NICER data suggest that the purely nucleonic composition may not be sufficient to describe the interiors of the NS.

In the right panel, the focus shifts to the frequency domain, analyzing the f -mode frequency determined using a linearized full General Relativity (GR) approach. In this analysis, the domain representing the entire nucleonic f -mode frequency is shown to be distinctly different from the constraints inferred by NICER, considering the aforementioned correlation. However, when the most probable region from the left panel is converted into the frequency domain through universal relation among the f -mode frequency and radius we obtained, it does not exclude the possibility of a nucleonic composition.

This suggests that while current data and methods do not rule out nucleonic compositions, future measurements of the f -mode frequency in NS, particularly those with extreme masses, have the potential to provide decisive evidence regarding the internal composition of NS. The implication is that such measurements could differentiate between purely nucleonic matter and other exotic phases, shedding light on the state of matter under extreme densities. For the first time, we have shown that the limitations derived from NICER in the frequency domain of the f -mode imply the necessity of

Empirical relation	Fitting function	Coefficients of current work	Relative error	Coefficients of (Pradhan et al. 2022)
$\frac{R^4}{M^3 \tau_f} - M/R$	$ax + b$	$a = -0.4286 \pm 0.0001$ $b = 0.1453 \pm 2.0 \times 10^{-5}$	0.19%	$a = -0.245$ $b = 0.080$

Table 3. Coefficients of the fitting equation for the empirical relations Eq.27

Empirical relation	Fitting function	Coefficients of current work	Relative error	Coefficients of (Kumar et al. 2023)
$f_{1.4} - R_{1.4}$	$ax + b$	$a = -0.1202 \pm 0.0007$ $b = 3.307 \pm 0.0096$	2.56%	$a = -0.22$ $b = 5.1$
$f_{2.0} - R_{2.0}$	$ax + b$	$a = -0.2367 \pm 0.0004$ $b = 4.948 \pm 0.0057$	2.22%	

Table 4. Coefficients of the fitting equation for the empirical relations Eq.28

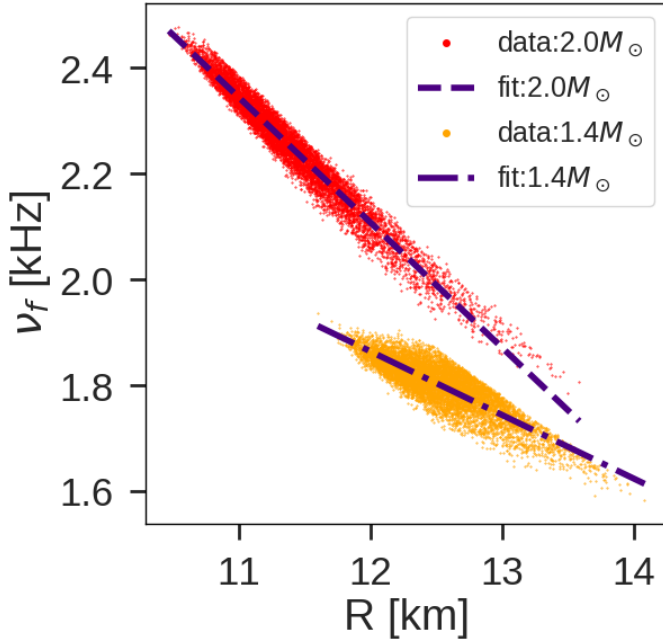


Figure 8. The empirical relation between the radii and the corresponding f -mode frequencies for the set of 9K RMF EOS used in this work. The orange(red) dots denote f -mode frequencies for NS with $1.4(2.0)M_{\odot}$. The dashed(dashed-dot) line represents the linear fit based on Eq. 28 for data for $1.4(2.0)M_{\odot}$.

considering other unusual degrees of freedom. Further observations may help to reveal this.

4. CONCLUSION

We have carefully calculated the quasinormal mode frequency, specifically focusing on the f -mode oscillations of NS. This analysis was conducted using a linearized approach to full General Relativity, which allowed for a detailed examination of these oscillations.

In our study, we utilized a wide range of nuclear EOS (9K), derived through Bayesian inference. These EOS were subjected to few constraints. Firstly, they conform to the minimal constraints on nuclear saturation properties. Secondly, they incorporate constraints from chiral effective field theory (χ EFT) relevant to low-density pure neutron matter. Additionally, constraints derived from perturbative Quantum Chromodynamics (pQCD) at densities pertinent to the core of NS were also applied. Finally, our selection of EOS ensured that the NS maximum mass was above $2M_{\odot}$, aligning with current astrophysical observations and theoretical predictions.

We then transformed the 9K EOS into a spectral representation of the EOS, which is the most widely accepted and optimal way to adapt any realistic EOS table into a functional form. This helps to reduce the computational time when calculating NS properties and is convenient for other astrophysical calculations. The mass-radius and mass-tidal deformability relationships of NS were calculated, and a detailed examination of the correlation among spectral parameters, various nuclear saturation properties and NS properties was conducted. Empirical relations for f -mode frequencies and gravitational wave damping times were also explored, providing valuable insights into the composition of these compact objects.

One of the key findings is that the f -mode frequencies do not show a strong relationship with any single nuclear saturation property of the EOS when the 9K EOS is used. In fact, we find that some of the strong correlations reported in recent publications have become weak for our EOS set. This observation suggests that a more nuanced approach, possibly involving multiparameter correlation analysis using machine learning techniques, might be necessary to unravel these complex relationships.

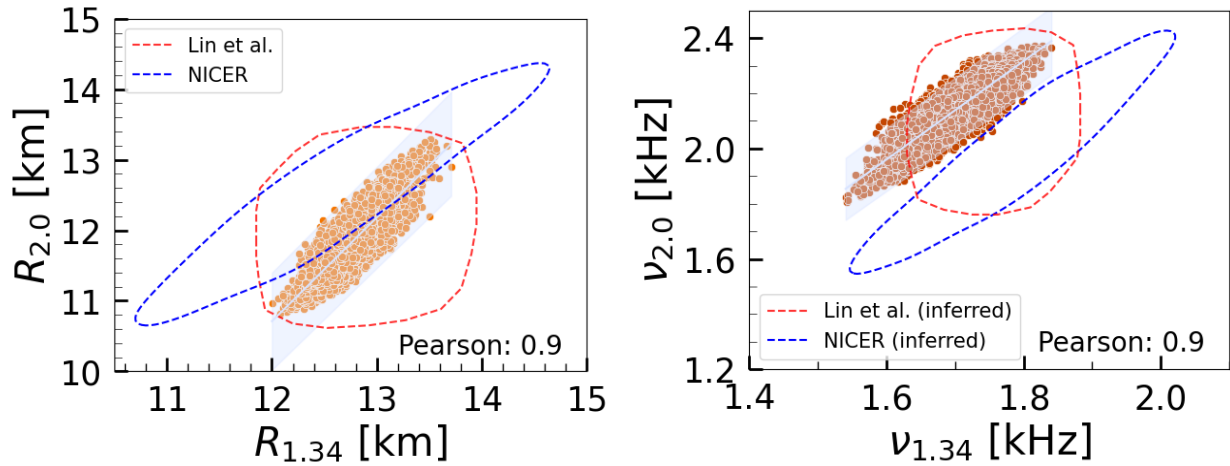


Figure 9. The relationship between the radii (left panel) and the f -mode frequencies (right panel) of NS(NS) with masses of $1.34M_{\odot}$ and $2.0M_{\odot}$ for the 9K nucleonic EOS used in this work. The dashed blue area on the left shows the NICER constraint, which was determined by taking the 1σ posteriors of the NICER measurements of PSR J0740+6620 and PSR 0030+0451 and marginalizing them over the NS mass while taking into account the correlation between them, based on the data in (Riley et al. 2019, 2021). The area shown in red dashed lines from the reference Lin & Steiner (2023) is the most likely area. On the right, we inferred this data in the frequency domain using the universal relation in Eq. 28 (see text for details).

Interestingly, a strong correlation was found among the radii and f -mode frequencies of the NS with extreme masses ($1.34M_{\odot}$ and $2.0M_{\odot}$). A recent study by Lin & Steiner (2023) combined the correlation between the radii with the NICER observation data and proposed the possibility of a phase transition in the EOS. However, our analysis suggests that the joint posterior of NICER calculated in that article completely overlaps with our entire EOS set employed with only nucleonic composition. However, if we impose the obtained correlation among the NS radii and the f -mode frequency for different masses on the NICER data, then it has minimal overlap in the radius domain and differs in the frequency domain with our entire EOS set. This suggests the possibility that additional, perhaps exotic, elements could be present in the core of NS. In the future, a detailed analysis is needed to determine the correlation and slope of the radius and the frequency of the extreme mass mode f for different configurations of EOS com-

position with a wide range of EOS. This research has a major impact on our understanding of NS and provides a basis for further investigations that seek to unravel the secrets of these remarkable celestial bodies.

ACKNOWLEDGMENTS

T.M. would like to acknowledge the support by national funds from FCT (Fundação para a Ciência e a Tecnologia, IEP, Portugal) under Projects No. UIDP/-04564/-2020, No. UIDB/-04564/-2020, and 2022.06460.PTDC. T.M. is grateful for the support of EURO-LABS "EUROpean Laboratories for Accelerator Based Science", which was funded by the Horizon Europe research and innovation programme with grant agreement No. 101057511. D. G. R., Sw.B., and Sa.B. would like to acknowledge the financial support by DST-SERB, Govt. of India through the Core Research Grant (CRG/2020/003899) for the project entitled: 'Investigating the Equation of State of Neutron Stars through Gravitational Wave Emission'.

REFERENCES

- Abbott, B., Abbott, R., Abbott, T., et al. 2018, Physical Review Letters, 121, doi: [10.1103/physrevlett.121.161101](https://doi.org/10.1103/physrevlett.121.161101)
- . 2019, Physical Review X, 9, doi: [10.1103/physrevx.9.011001](https://doi.org/10.1103/physrevx.9.011001)
- Agrawal, B. K., Malik, T., De, J. N., & Samaddar, S. K. 2021, The European Physical Journal Special Topics, doi: [10.1140/epjs/s11734-021-00001-7](https://doi.org/10.1140/epjs/s11734-021-00001-7)
- Andersson, N. 2019, Gravitational-Wave Astronomy (Oxford University Press), doi: [10.1093/oso/9780198568032.001.0001](https://doi.org/10.1093/oso/9780198568032.001.0001)
- . 2021, Universe, 7, 97, doi: [10.3390/universe7040097](https://doi.org/10.3390/universe7040097)
- Andersson, N., & Kokkotas, K. D. 1996, Physical Review Letters, 77, 4134, doi: [10.1103/physrevlett.77.4134](https://doi.org/10.1103/physrevlett.77.4134)
- . 1998, Monthly Notices of the Royal Astronomical Society, 299, 1059, doi: [10.1046/j.1365-8711.1998.01840.x](https://doi.org/10.1046/j.1365-8711.1998.01840.x)

- Andersson, N., & Pnigouras, P. 2020, *Physical Review D*, 101, 083001
- . 2021, *Monthly Notices of the Royal Astronomical Society*, 503, 533, doi: [10.1093/mnras/stab371](https://doi.org/10.1093/mnras/stab371)
- Antoniadis, J., Freire, P. C. C., Wex, N., et al. 2013, *Science*, 340, doi: [10.1126/science.1233232](https://doi.org/10.1126/science.1233232)
- Banik, S., Hempel, M., & Bandyopadhyay, D. 2014, *The Astrophysical Journal Supplement Series*, 214, 22, doi: [10.1088/0067-0049/214/2/22](https://doi.org/10.1088/0067-0049/214/2/22)
- Baym, G., Pethick, C., & Sutherland, P. 1971, *The Astrophysical Journal*, 170, 299, doi: [10.1086/151216](https://doi.org/10.1086/151216)
- Benhar, O., Ferrari, V., & Gualtieri, L. 2004, *Physical Review D*, 70, doi: [10.1103/physrevd.70.124015](https://doi.org/10.1103/physrevd.70.124015)
- Branchesi, M., Maggiore, M., Alonso, D., et al. 2023, *Journal of Cosmology and Astroparticle Physics*, 2023, 068, doi: [10.1088/1475-7516/2023/07/068](https://doi.org/10.1088/1475-7516/2023/07/068)
- Chan, T., Sham, Y.-H., Leung, P., & Lin, L.-M. 2014, *Physical Review D*, 90, 124023
- Char, P., Banik, S., & Bandyopadhyay, D. 2015, *The Astrophysical Journal*, 809, 116, doi: [10.1088/0004-637x/809/2/116](https://doi.org/10.1088/0004-637x/809/2/116)
- Cromartie, H. T., Fonseca, E., Ransom, S. M., et al. 2019, *Nature Astronomy*, 4, 72–76, doi: [10.1038/s41550-019-0880-2](https://doi.org/10.1038/s41550-019-0880-2)
- Demorest, P. B., Pennucci, T., Ransom, S. M., Roberts, M. S. E., & Hessels, J. W. T. 2010, *Nature*, 467, 1081–1083, doi: [10.1038/nature09466](https://doi.org/10.1038/nature09466)
- Detweiler, S. L. 1975, *Astrophysical Journal*, vol. 197, Apr. 1, 1975, pt. 1, p. 203–217., 197, 203
- Doneva, D. D., Gaertig, E., Kokkotas, K. D., & Krüger, C. 2013, *Physical Review D*, 88, doi: [10.1103/physrevd.88.044052](https://doi.org/10.1103/physrevd.88.044052)
- Dutra, M., Lourenço, O., Avancini, S. S., et al. 2014, *Physical Review C*, 90, doi: [10.1103/physrevc.90.055203](https://doi.org/10.1103/physrevc.90.055203)
- Fonseca, E., Cromartie, H. T., Pennucci, T. T., et al. 2021, *The Astrophysical Journal Letters*, 915, L12, doi: [10.3847/2041-8213/ac03b8](https://doi.org/10.3847/2041-8213/ac03b8)
- Greif, S. K., Raaijmakers, G., Hebel, K., Schwenk, A., & Watts, A. L. 2019, *Monthly Notices of the Royal Astronomical Society*, 485, 5363–5376, doi: [10.1093/mnras/stz654](https://doi.org/10.1093/mnras/stz654)
- Hebel, K., Lattimer, J. M., Pethick, C. J., & Schwenk, A. 2010, *Physical Review Letters*, 105, doi: [10.1103/physrevlett.105.161102](https://doi.org/10.1103/physrevlett.105.161102)
- Kokkotas, K., Apostolatos, T., & Andersson, N. 2001, *Monthly Notices of the Royal Astronomical Society*, 320, 307
- Kokkotas, K. D., & Schmidt, B. G. 1999, *Living Reviews in Relativity*, 2, 2, doi: [10.12942/lrr-1999-2](https://doi.org/10.12942/lrr-1999-2)
- Komoltsev, O., & Kurkela, A. 2022, *Physical Review Letters*, 128, doi: [10.1103/physrevlett.128.202701](https://doi.org/10.1103/physrevlett.128.202701)
- Kumar, D., Malik, T., Mishra, H., & Providência, C. 2023, *Physical Review D*, 108, doi: [10.1103/physrevd.108.083008](https://doi.org/10.1103/physrevd.108.083008)
- Kunjipurayil, A., Zhao, T., Kumar, B., Agrawal, B. K., & Prakash, M. 2022, *Physical Review D*, 106, doi: [10.1103/physrevd.106.063005](https://doi.org/10.1103/physrevd.106.063005)
- Kurkela, A., Romatschke, P., & Vuorinen, A. 2010, *Physical Review D*, 81, doi: [10.1103/physrevd.81.105021](https://doi.org/10.1103/physrevd.81.105021)
- Lattimer, J., & Prakash, M. 2001, *The Astrophysical Journal*, 550, 426
- Lau, H., Leung, P., & Lin, L. 2010, *The Astrophysical Journal*, 714, 1234
- Leins, M., Nollert, H. P., & Soffel, M. H. 1993, *Physical Review D*, 48, 3467, doi: [10.1103/physrevd.48.3467](https://doi.org/10.1103/physrevd.48.3467)
- Lin, Z., & Steiner, A. 2023, *Indication of Sharp and Strong Phase-Transitions from NICER Observations*, arXiv, doi: [10.48550/ARXIV.2310.01619](https://doi.org/10.48550/ARXIV.2310.01619)
- Lindblom, L. 2010, *Physical Review D*, 82, doi: [10.1103/physrevd.82.103011](https://doi.org/10.1103/physrevd.82.103011)
- . 2018, *Physical Review D*, 97, doi: [10.1103/physrevd.97.123019](https://doi.org/10.1103/physrevd.97.123019)
- . 2022, *Physical Review D*, 105, doi: [10.1103/physrevd.105.063031](https://doi.org/10.1103/physrevd.105.063031)
- Lindblom, L., & Detweiler, S. L. 1983, *The Astrophysical Journal Supplement Series*, 53, 73, doi: [10.1086/190884](https://doi.org/10.1086/190884)
- Malik, T., Banik, S., & Bandyopadhyay, D. 2021, *The Astrophysical Journal*, 910, 96, doi: [10.3847/1538-4357/abe860](https://doi.org/10.3847/1538-4357/abe860)
- Malik, T., Ferreira, M., Albino, M. B., & Providência, C. 2023, *Physical Review D*, 107, doi: [10.1103/physrevd.107.103018](https://doi.org/10.1103/physrevd.107.103018)
- Miller, M. C., Lamb, F. K., Dittmann, A. J., et al. 2019, *The Astrophysical Journal*, 887, L24, doi: [10.3847/2041-8213/ab50c5](https://doi.org/10.3847/2041-8213/ab50c5)
- . 2021, *The Astrophysical Journal Letters*, 918, L28, doi: [10.3847/2041-8213/ac089b](https://doi.org/10.3847/2041-8213/ac089b)
- Nandi, R., Char, P., & Pal, S. 2019, *Physical Review C*, 99, doi: [10.1103/physrevc.99.052802](https://doi.org/10.1103/physrevc.99.052802)
- O’Boyle, M. F., Markakis, C., Stergioulas, N., & Read, J. S. 2020, *Physical Review D*, 102, doi: [10.1103/physrevd.102.083027](https://doi.org/10.1103/physrevd.102.083027)
- Patra, N. K., Venneti, A., Imam, S. M. A., Mukherjee, A., & Agrawal, B. K. 2023, *Physical Review C*, 107, doi: [10.1103/physrevc.107.055804](https://doi.org/10.1103/physrevc.107.055804)
- Poisson, E., & Will, C. M. 2014, *Gravity: Newtonian, post-newtonian, relativistic* (Cambridge University Press)

- Pradhan, B. K., Chatterjee, D., Lanoye, M., & Jaikumar, P. 2022, *Physical Review C*, 106, doi: [10.1103/physrevc.106.015805](https://doi.org/10.1103/physrevc.106.015805)
- Pradhan, B. K., Pathak, D., & Chatterjee, D. 2023, *The Astrophysical Journal*, 956, 38, doi: [10.3847/1538-4357/acef1f](https://doi.org/10.3847/1538-4357/acef1f)
- Pratten, G., Schmidt, P., & Hinderer, T. 2020, *Nature communications*, 11, 2553
- Raaijmakers, G., Greif, S. K., Riley, T. E., et al. 2020, *The Astrophysical Journal*, 893, L21, doi: [10.3847/2041-8213/ab822f](https://doi.org/10.3847/2041-8213/ab822f)
- Regge, T., & Wheeler, J. A. 1957, *Phys. Rev.*, 108, 1063, doi: [10.1103/PhysRev.108.1063](https://doi.org/10.1103/PhysRev.108.1063)
- Reisenegger, A., & Goldreich, P. 1992, *The Astrophysical Journal*, 395, 240, doi: [10.1086/171645](https://doi.org/10.1086/171645)
- Rezzolla, L. 2003, *Gravitational Waves from Perturbed Black Holes and Relativistic Stars*, arXiv, doi: [10.48550/ARXIV.GR-QC/0302025](https://doi.org/10.48550/ARXIV.GR-QC/0302025)
- Rezzolla, L., Most, E. R., & Weih, L. R. 2018, *The Astrophysical Journal*, 852, L25, doi: [10.3847/2041-8213/aaa401](https://doi.org/10.3847/2041-8213/aaa401)
- Riley, T. E., Watts, A. L., Bogdanov, S., et al. 2019, *The Astrophysical Journal*, 887, L21, doi: [10.3847/2041-8213/ab481c](https://doi.org/10.3847/2041-8213/ab481c)
- Riley, T. E., Watts, A. L., Ray, P. S., et al. 2021, *The Astrophysical Journal Letters*, 918, L27, doi: [10.3847/2041-8213/ac0a81](https://doi.org/10.3847/2041-8213/ac0a81)
- Servignat, G., Davis, P. J., Novak, J., Oertel, M., & Pons, J. A. 2023, One- and two-parameter equation of state parametrizations with continuous sound speed for neutron star simulations, arXiv, doi: [10.48550/ARXIV.2311.02653](https://doi.org/10.48550/ARXIV.2311.02653)
- Sotani, H. 2021, *Physical Review D*, 103, doi: [10.1103/physrevd.103.123015](https://doi.org/10.1103/physrevd.103.123015)
- Sotani, H., & Takiwaki, T. 2020, *Phys. Rev. D*, 102, 063025, doi: [10.1103/PhysRevD.102.063025](https://doi.org/10.1103/PhysRevD.102.063025)
- Sotani, H., Tominaga, K., & ichi Maeda, K. 2001, *Physical Review D*, 65, doi: [10.1103/physrevd.65.024010](https://doi.org/10.1103/physrevd.65.024010)
- Tews, I., Carlson, J., Gandolfi, S., & Reddy, S. 2018, *The Astrophysical Journal*, 860, 149, doi: [10.3847/1538-4357/aac267](https://doi.org/10.3847/1538-4357/aac267)
- Thorne, K. S., & Campolattaro, A. 1967, *The Astrophysical Journal*, 149, 591, doi: [10.1086/149288](https://doi.org/10.1086/149288)
- Tsui, L., & Leung, P. 2005, *Monthly Notices of the Royal Astronomical Society*, 357, 1029
- Vishveshwara, C. V. 1970, *Nature*, 227, 936, doi: [10.1038/227936a0](https://doi.org/10.1038/227936a0)
- Walecka, J. 1974, *Annals of Physics*, 83, 491–529, doi: [10.1016/0003-4916\(74\)90208-5](https://doi.org/10.1016/0003-4916(74)90208-5)
- Yagi, K., & Yunes, N. 2013, *Science*, 341, 365
- Zerilli, F. J. 1970, *Phys. Rev. Lett.*, 24, 737, doi: [10.1103/PhysRevLett.24.737](https://doi.org/10.1103/PhysRevLett.24.737)